

Exotic surface states in hybrid structures of topological insulators and Weyl semimetals

Stefan Juergens and Björn Trauzettel
*Institute of Theoretical Physics and Astrophysics,
 University of Würzburg, D-97074 Würzburg, Germany*
 (Dated: May 20, 2022)

Topological insulators (TIs) and Weyl semimetals (WSMs) are two realizations of topological matter usually appearing separate in nature, but directly related to each other via a phase transition. In this paper, we investigate the question whether these two topological phases can exist together at the same time, with a combined, hybrid surface state at the joint boundaries. We analyze effective models of a 3D TI and an inversion symmetric WSM and couple them in a way that certain symmetries, like inversion, are preserved. A tunnel coupling approach enables us to obtain the hybrid surface state Hamiltonian analytically. This offers the possibility of a detailed study of its dispersion depending on the investigated couplings. For spin-symmetric coupling, we find that two Dirac nodes can emerge out of the combination of a single Dirac node and a Fermi arc. For spin-asymmetric coupling, the dispersion is gapped and the former Dirac node gets spin-polarized. We present different experimental realization of the hybrid system, including compressively strained HgTe as well as heterostructures of TI and WSM materials.

PACS numbers:

I. INTRODUCTION

The study of topological properties in a semiconductor environment has become a strong and flourishing field in condensed matter physics. Topological insulators (TIs) are the standard materials in this context, well studied both theoretically and experimentally by now¹⁻³. Their semi-metallic cousins, Weyl semimetals (WSMs)⁴⁻⁷, were proposed to exist in condensed matter systems decades ago⁸⁻¹⁰. However, only very recently with the prediction of concrete material realizations¹¹⁻¹³ the field has seen an enormous growth. The experimental proof of the existence of Weyl points and their corresponding surface states, called Fermi arcs, followed soon afterwards¹⁴⁻¹⁹. Yet both for fundamental research and application purposes these "early" WSM, like the TaAs family of non-centrosymmetric monpnictides, are too complicated with many Weyl points (24 for TaAs) in the Brillouin zone. Simpler materials with 8²⁰⁻²⁹ and 4^{30,31} Weyl points have been predicted and observed, where the latter is the minimal number of Weyl points for a system with time-reversal symmetry (TRS). Materials with broken TRS³² could realize the absolute minimum of 2 Weyl points, but for that case only theoretical proposals³³⁻³⁷ exist so far. Most of them rely on magnetically doped TIs or TI heterostructures.

TI and WSM are both topological phases that can be directly connected to each other through quantum phase transitions^{10,38}. In this paper we want to go a step further and study the question whether a system can be both in the TI and WSM phase at the same time, or at least support both corresponding surface states, the Dirac states and the Fermi arcs, on the same surface.

Such a combined phase might exist in HgTe with applied compressive strain. The strain pushes the Γ_8 bands into one another, creating Dirac points which are then

split by breaking of inversion symmetry through bulk inversion asymmetry (BIA) terms²⁶. At the same time, the topological band inversion between the Γ_8 and the Γ_6 bands remains, leading to the conjecture that this system could have topological Dirac states and Fermi arcs on its surface.

A different way to create such a hybrid surface state is placing a TI and WSM spatially adjacent to each other, possibly separated by a small, topological trivial buffer layer. The separate surface states of TI and WSM will interact, e.g. by Coulomb interaction or tunneling due to a small overlap of wave functions, forming the hybrid surface dispersion. Previous related research on adjacent TI and WSM phases³⁹ suggest that at such a shared surface both Dirac states and Fermi arcs can exist. However, they were found in different areas of k-space, mutually excluding one another such that they do not hybridize at all. Our approach differs from this one by considering only a small, perturbative coupling between the two phases. This ensures that both TI and WSM surface states survive and can interact with each other.

We focus in this paper on an analytical study of the combined surface states generated from the hybridized TI and WSM. A simplified Ansatz offers the possibility to calculate the surface Hamiltonian analytically, allowing for a detailed analysis of the surface physics. Depending on the symmetry of the assumed couplings, the surface dispersion shows quite different behaviour. In the case of spin symmetry, two shifted Dirac nodes may emerge out of the combination of a single Dirac node and a Fermi arc. For spin-asymmetric coupling, the Fermi arc gaps out and spin-polarizes the former Dirac node.

The article is organized as follows. We recap effective models for the separate phases of TI and WSM^{38,40-43} and discuss their symmetry properties and surface states in Sec. II. The coupling of the Hamiltonians and the an-

alytic form of the surface state is discussed in Sec. III. Sec. IV focuses on the different ways to influence and tune the combined surface dispersion. Possible experimental realizations are proposed in Sec. V.

II. SEPARATE MODELS

The model of the TI phase we will use was originally derived for the Bi_2Se_3 family of materials in Refs. 40, 41. It contains four bands and serves as a minimal, but general, TI model. The Weyl Hamiltonian considered in the following originates from Refs. 42,43. It contains two bands and models an inversion symmetric type I or II WSM with two Weyl points. We simplify the models as far as possible without losing too much versatility. It is important to retain terms quadratic in momentum for the introduction of the surface in z direction. This is done via hardwall boundary conditions on a half space $z \leq 0$ or $z \geq 0$.

A. Topological Insulator

The effective Hamiltonian for a 3D TI is given by the 4x4 matrix^{40,41}

$$H_{TI} = \begin{pmatrix} M(k)\tau_3 + Bk_z\tau_2 + C\tau_0 & iAk_-\tau_1 \\ -iA^*k_+\tau_1 & M(k)\tau_3 + Bk_z\tau_2 + C\tau_0 \end{pmatrix} \quad (2.1)$$

with $M(k) = M_0 + M_1(k_{\parallel}^2 + k_z^2)$, $k_{\parallel}^2 = k_x^2 + k_y^2$ and $k_{\pm} = k_x \pm ik_y = k_{\parallel}e^{\pm i\phi_k}$. In the original derivation for Bi_2Se_3 the Pauli matrices $\vec{\tau}$ describe an orbital degree of freedom. H_{TI} is written in a spin up / down basis, represented by the Pauli matrices $\vec{\sigma}$ in the following. The coupling $A = |A|e^{i\phi_A}$ can be complex. The model is in the strong TI phase for $M_0M_1 < 0$.

We define the inversion operator $P_{TI} = \sigma_0 \otimes \tau_3$ and time-reversal operator $T_{TI} = i\sigma_2 \otimes \tau_0 K$ with K the complex conjugation operator. H_{TI} is symmetric under both operations, fulfilling

$$\begin{aligned} P_{TI}^\dagger H_{TI}(-k) P_{TI} &= H_{TI}(k) \\ T_{TI}^\dagger H_{TI}(-k) T_{TI} &= H_{TI}(k). \end{aligned} \quad (2.2)$$

The bulk dispersion is double degenerate and given by

$$E_{TI} = C \pm \sqrt{|A|^2 k_{\parallel}^2 + B^2 k_z^2 + M(k)^2}. \quad (2.3)$$

Based on the method described in the App. A the surface states can be calculated analytically. We assume opposite surfaces to be well separated, which offers the possibility to treat them individually. Thus in the calculation we only consider one of them via hardwall boundary conditions at $z = 0$. The surface wave function is then given by

$$\Psi(z) = \frac{1}{\sqrt{2}} (e^{ik_z,1z} - e^{ik_z,2z}) \begin{pmatrix} \pm \frac{i\eta A k_-}{|A|k_{\parallel}} \psi_{\eta} \\ \psi_{\eta} \end{pmatrix} \quad (2.4)$$

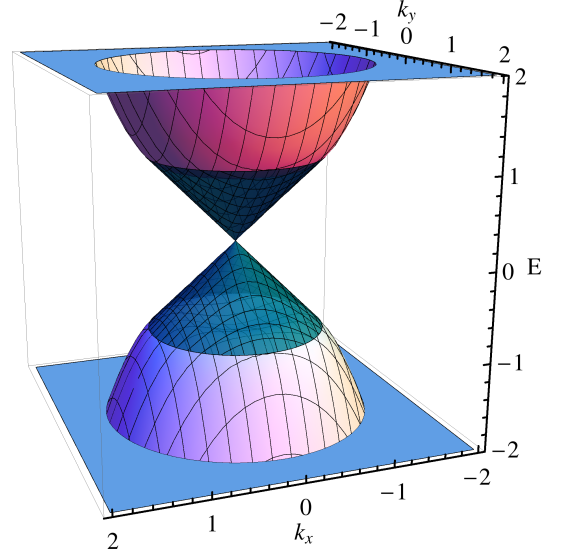


FIG. 1: Bulk and surface (cyan) dispersion, Eq. (2.3) and Eq. (2.6), of the TI model.

Parameters: $C = 0$, $M_0 = -1$, $M_1 = 1$, $A = 1$, $B = 1$, $k_z = 0$.

with $\psi_{\eta} = \frac{1}{\sqrt{2}} \begin{pmatrix} 1 \\ \eta \end{pmatrix}$ and the inverse localization length $ik_z = \frac{1}{2M_1} \left(-\eta B \pm \sqrt{4M_1(M_0 + M_1 k_{\parallel}^2) + B^2} \right)$. The sign $\eta = \pm$ depends on the surface, $\eta = -\text{sgn}\left(\frac{B}{M_1}\right)$ (upper surface) or $\eta = \text{sgn}\left(\frac{B}{M_1}\right)$ (lower surface).

The existence condition for the surface state is

$$M_1(M_0 + M_1 k_{\parallel}^2) < 0 \quad (2.5)$$

stressing the importance of being in the inverted regime.

The surface Hamiltonian (dispersion) is obtained from H_{TI} by projecting out the orbital (orbital & spin) degrees of freedom with the help of $\psi_{\eta}(\Psi(z))$. We find the usual Dirac form

$$H_{TI}^{sur} = \begin{pmatrix} C & i\eta A k_- \\ -i\eta A^* k_+ & C \end{pmatrix}; \quad E_{TI}^{sur} = C \pm |A|k_{\parallel}, \quad (2.6)$$

experiencing spin-momentum locking, with the angle $\phi_A + \frac{\eta\pi}{2}$ between the spin projection and momentum vector in the x-y plane. The combined dispersions of bulk and surface of the TI are shown in Fig. 1.

B. Inversion symmetric Weyl Semimetal

A WSM exists in different flavors. On the one hand, one distinguishes type I and type II depending on preserved or broken Lorentz invariance at the Weyl points^{44,45}. Secondly, either time-reversal or inversion symmetry has to be broken to get from a Dirac to a Weyl semimetal. For all these phases minimal models have been proposed in the literature^{38,42,43,46}.

For simplicity, we focus on the model with broken time-reversal and preserved inversion symmetry, as it has the minimal number of one pair of Weyl points. The Hamiltonian is

$$H_W = t(k)\tau_3 + v_z k_z \tau_2 + v_y k_y \tau_1 + \gamma t(k_x^2 - k_W^2) \tau_0 \quad (2.7)$$

with $t(k) = t(k_{\parallel}^2 + k_z^2 - k_W^2)$. The degree of freedom described by the Pauli matrices $\vec{\tau}$ can be orbital, spin or a combination of the two, depending on the specific material realization. For the concrete form of the symmetry operations considered in the following we assume a spinless system⁴³. The two Weyl points are specified by $k_x = \pm k_W$. The parameter γ leads to a tilting of the dispersion at the Weyl points. For $|\gamma| < 1$ one has a type I, otherwise a type II WSM. Expanding H_W around $k_x = \pm k_W$ gives the linearized Weyl dispersion

$$E_W^{lin} = v_y k_y \tau_1 + v_z k_z \tau_2 \pm 2t k_W k_x (\tau_3 + \gamma \tau_0). \quad (2.8)$$

The Hamiltonian H_W fulfills the symmetry conditions

$$\begin{aligned} P_W^\dagger H_W(-k) P_W &= H_W(k) \\ T_W^\dagger H_W(-k) T_W &\neq H_W(k) \end{aligned} \quad (2.9)$$

with the inversion operator $P_W = \tau_3$ and time-reversal operator $T_W = \tau_0 K$ with K the complex conjugation operator. Hence, parity is preserved and time-reversal symmetry broken.

The bulk dispersion is then given by

$$E_W = \gamma t(k_x^2 - k_W^2) \pm \sqrt{v_y^2 k_y^2 + v_z^2 k_z^2 + t(k)^2}. \quad (2.10)$$

The surface states can be calculated analytically based on the method discussed in the App. A. Their wave function is given by

$$\Psi(z) = (e^{ik_{z,1}z} - e^{ik_{z,2}z}) \psi_\eta \quad (2.11)$$

with $\psi_\eta = \frac{1}{\sqrt{2}} \begin{pmatrix} 1 \\ \eta \end{pmatrix}$ and inverse localization length $ik_z = \frac{1}{2t} \left(-\eta v_z \pm \sqrt{4t^2(k_{\parallel}^2 - k_W^2) + v_z^2} \right)$. The sign $\eta = \pm$ depends on the surface, $\eta = -\text{sgn}(\frac{v_z}{t})$ (upper surface) or $\eta = \text{sgn}(\frac{v_z}{t})$ (lower surface).

The existence condition for the surface state is

$$k_{\parallel}^2 < k_W^2 \quad (2.12)$$

such that Fermi arcs can only exist between the Weyl points.

Hence, the surface dispersion yields the known Fermi arc spectrum

$$E_W^{sur} = \gamma t(k_x^2 - k_W^2) + \eta v_y k_y. \quad (2.13)$$

The combined dispersions of bulk and surface of the WSM are shown in Fig. 2.

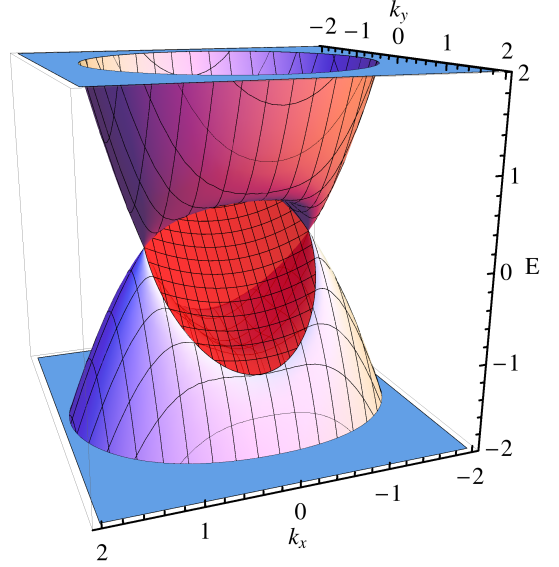


FIG. 2: Bulk and upper surface (red) dispersion, Eq. (2.10) and Eq. (2.13), of the Weyl model.

Parameters: $\gamma = \frac{1}{4}$, $k_W = 1$, $t = 1$, $v_y = 1$, $v_z = 1$, $k_z = 0$.

III. COUPLED SYSTEM

The Hamiltonians and surface wave functions of the TI and WSM phases discussed in Sec. II are very similar. Thus, we hope that also the combined system may have surface states which can be calculated by the simplified method described in App. A. This will allow us to discuss the surface physics analytically.

In this section, we define the combined Hamiltonian and discuss the couplings allowed by symmetry under the assumptions that certain symmetries are preserved. The surface state Hamiltonian and wave function are derived and the limitations due to the approximated calculation method are discussed.

The combined Hamiltonian of TI and WSM phase is defined by

$$H_{WTI} = \begin{pmatrix} H_{TI} & H_C \\ H_C^\dagger & H_W \end{pmatrix} \quad (3.1)$$

with the coupling H_C . Such a coupling can be regarded as a tunneling Hamiltonian approach where H_C (weakly) couples the two entities H_{TI} and H_W . The combined symmetry operator for inversion symmetry is given by

$$P_{WTI} = \begin{pmatrix} P_{TI} & 0 \\ 0 & P_W \end{pmatrix}. \quad (3.2)$$

As time-reversal symmetry is already broken in the subsystem of the WSM, it will also be absent in the combined system. Applying the inversion operator to the Hamiltonian, following Eqs. (2.2), (2.9), yields restrictions for the allowed couplings assuming that this symmetry is not broken. As the symmetry operator is block-diagonal, these restrictions do not depend on H_W or H_{TI} .

For an inversion symmetric system, the couplings proportional to τ_3 and τ_0 have to be even in momentum, while the ones proportional to τ_2 and τ_1 have to be odd in momentum. We choose the following representation

$$H_{C,IS} = \begin{pmatrix} H_{c,IS} \\ \tilde{H}_{c,IS} \end{pmatrix} \quad (3.3)$$

with

$$H_{c,IS} = d(k_{\parallel})\tau_3 + c_1k_+\tau_2 + b_1k_+\tau_1 + a(k_{\parallel})\tau_0, \quad (3.4)$$

where $d(k_{\parallel}) = d_0 + d_2k_{\parallel}^2$, $a(k_{\parallel}) = a_0 + a_2k_{\parallel}^2$, and $\tilde{H}_{c,IS}$ having the same structure. This choice ensures the preservation of parity for the combined system. Coupling terms proportional to k_z are not considered, for simplicity. This is a physically reasonable assumption at least for the surface states if one assumes them to be 2D, perfectly localized in z -direction. Close to the Weyl points or the TI bulk band edge where the surface states delocalize a k_z dependent coupling should be taken into account.

The Ansatz we will consider is

$$\Psi(z) = (e^{ik_z,1z} - e^{ik_z,2z}) \begin{pmatrix} L_1(k_{\pm}) \psi_{\eta_{TI}} \\ L_2(k_{\pm}) \psi_{\eta_{TI}} \\ L_3(k_{\pm}) \psi_{\eta_W} \end{pmatrix} \quad (3.5)$$

with $\psi_{\eta} = \frac{1}{\sqrt{2}} \begin{pmatrix} 1 \\ \eta \end{pmatrix}$. This is a special case of the general form of the surface wave function $\Psi_g(z) = \sum_j a_j e^{ik_{z,j}z} \psi(k_{\pm}, k_{z,j})$, $j \in \{1, \dots, 6\}$. Its choice is motivated by the ability to obtain analytical solutions for the surface states. Physically it means that we only consider solutions where the TI and WSM surface states have the same exponential localization with the same localization length. This implies that phase transitions of the subsystems, like normal insulator (NI) to TI or NI to WSM, can not be discussed separately in this treatment. However, for a system deep in the TI and WSM phase, the simplification should not alter the essential physics.

Projecting the Hamiltonian Eq. (3.1) on the surface, this separates the eigenvalue equation into simpler problems

$$H_{WTI}^{sur} \begin{pmatrix} L1 \\ L2 \\ L3 \end{pmatrix} = E_{WTI}^{sur} \begin{pmatrix} L1 \\ L2 \\ L3 \end{pmatrix} \quad (3.6)$$

$$H_{WTI}^{k_z} \begin{pmatrix} L1 \\ L2 \\ L3 \end{pmatrix} = 0 \quad (3.7)$$

with the Hamiltonians

$$H_{WTI}^{sur} = \begin{pmatrix} C & i\eta A k_- & a(k_{\parallel}) + \eta b_1 k_+ \\ -i\eta A^* k_+ & C & \tilde{a}(k_{\parallel}) + \eta \tilde{b}_1 k_+ \\ a(k_{\parallel})^* + \eta b_1^* k_- & \tilde{a}(k_{\parallel})^* + \eta \tilde{b}_1^* k_- & \gamma t(k_x^2 - k_W^2) + \eta v_y k_y \end{pmatrix} \quad (3.8)$$

$$\xRightarrow{\text{part. diag.}} \begin{pmatrix} C + |A| k_{\parallel} & 0 & \tilde{H}_c + e^{i\phi_k^A} H_c \\ 0 & C - |A| k_{\parallel} & \tilde{H}_c - e^{i\phi_k^A} H_c \\ \tilde{H}_c^* + e^{-i\phi_k^A} H_c^* & \tilde{H}_c - e^{-i\phi_k^A} H_c^* & \gamma t(k_x^2 - k_W^2) + \eta v_y k_y \end{pmatrix} \quad (3.9)$$

$$H_{WTI}^{k_z} = \begin{pmatrix} M(k) - i\eta B k_z & 0 & d(k_{\parallel}) - i\eta c_1 k_+ \\ 0 & M(k) - i\eta B k_z & \tilde{d}(k_{\parallel}) - i\eta \tilde{c}_1 k_+ \\ d(k_{\parallel})^* - i\eta c_1^* k_- & \tilde{d}(k_{\parallel})^* - i\eta \tilde{c}_1^* k_- & t(k) - i\eta v_z k_z \end{pmatrix} \quad (3.10)$$

for $\eta = \eta_{TI} = \eta_W$. In Eq. (3.9), we partially diagonalize the Hamiltonian and define $\phi_k^A = \phi_k - \phi_A - \eta \frac{\pi}{2}$, $H_c = a(k_{\parallel}) + \eta b_1 k_+$ and $\tilde{H}_c = \tilde{a}(k_{\parallel}) + \eta \tilde{b}_1 k_+$. In the case of $\eta = \eta_{TI} = -\eta_W$, one changes in Eqs. (3.8) - (3.10) $a(k_{\parallel}) \leftrightarrow d(k_{\parallel})$, $b_1 \leftrightarrow i c_1$, $v_y \rightarrow -v_y$ and $v_z \rightarrow -v_z$. We will focus in the following on the former, $\eta_{TI} = \eta_W$, case. Taking $(L1 \ L2 \ L3)^T$ as the eigenvector in Eq. (3.6), Eq. (3.7) can only be fulfilled by further restrictions on the parameters. We choose a locking between some of the TI and the WSM parameters, i.e. $t(k) = \nu M(k)$ and $v_z = \nu B$ with ν a constant (set to 1 in the following). This ensures the same localization length for the two subsystems. Additionally, the couplings c_1 and $d(k_{\parallel})$ are set to be 0. Therefore the total coupling does

not change the original orbital character of the TI and WSM surface states, being eigenstates of the τ_1 matrix with fixed eigenvalue $+$ or $-$. In total, this leads to the same quadratic equation for k_z as in the pure TI case, $ik_z = \frac{1}{2M_1} \left(-\eta B \pm \sqrt{4M_1 (M_0 + M_1 k_{\parallel}^2) + B^2} \right)$. The existence condition is again

$$M_1 (M_0 + M_1 k_{\parallel}^2) < 0 \quad (3.11)$$

and the (unnormalized) eigenvectors are given by

$$\begin{pmatrix} L1 \\ L2 \\ L3 \end{pmatrix} = \begin{pmatrix} (E_{WTI}^{sur} - C) H_c + i\eta A k_- \tilde{H}_c \\ (E_{WTI}^{sur} - C) \tilde{H}_c - i\eta A^* k_+ H_c \\ (E_{WTI}^{sur} - C)^2 - |A|^2 k_{\parallel}^2 \end{pmatrix}. \quad (3.12)$$

The eigenenergies $E_{W_{TI}}^{sur}$ are too lengthy to state them here, but can also be derived analytically.

The obtained solution leads to the possibility to tune bulk and surface dispersions rather independently. Parameters M_i and B influence the surface dispersion only indirectly via the existence condition and finite γ parameter, while they strongly influence the bulk band structure as will be shown in the next section. Tuning the coupling constants v_y , A , $a(k_{\parallel})$, b_1 and their relative phase will still provide a rich parameter space to be explored below.

IV. SURFACE DISPERSION

In this section, we discuss the influence of the different coupling parameters on the combined surface states of TI and WSM. Depending on the symmetries of the coupling, observed phenomenas are the generation of additional Dirac points in the dispersion or the spin polarization of certain surface bands.

A. Uncoupled scenario

Beginning with the uncoupled case, $H_{C,IS} = 0$, the dispersion of the surface and bulk states are shown in Fig. 3. The black lines denote the bulk dispersion, cyan (from blue (green) for spin up (down)) and red stand for TI and WSM surface state, respectively. The two black dots give the position of the bulk Weyl points. We note that the surface states originate at the bulk states, but cross them unaffectedly. Together with the fact that one can tune the bulk gap M_0 without changing the surface dispersion (aside from the existence condition), we find the possibility to discuss bulk and surface dispersion rather separately from each other. It will always be possible to increase the bulk gap and the distance between the two Weyl points such that the interesting surface physics happens in regions of the Brillouin zone where no bulk state is located. Therefore, we will focus in the following on tuning of the surface dispersion only.

B. Real, spin-symmetric coupling: Creation of additional Dirac points

A straight forward way to couple TI and WSM is a real and spin-symmetric coupling via $a(k_{\parallel}) > 0$ or $b_1 > 0$ with $H_c = \tilde{H}_c$. This kind of coupling leads generally to two Dirac points in the combined surface dispersion, as plotted in Fig. 4. One Dirac point is just shifted by the coupling to the Weyl surface state. The other one is created out of the Weyl and Dirac states along a momentum direction where there is no coupling between these two bands. Under the assumption that both spin species couple equally strong to the WSM, $|\tilde{H}_c| = |H_c|$, there is always such a momentum direction ϕ_k where one part (hole or electron) of the Dirac cone is not coupled to the WSM

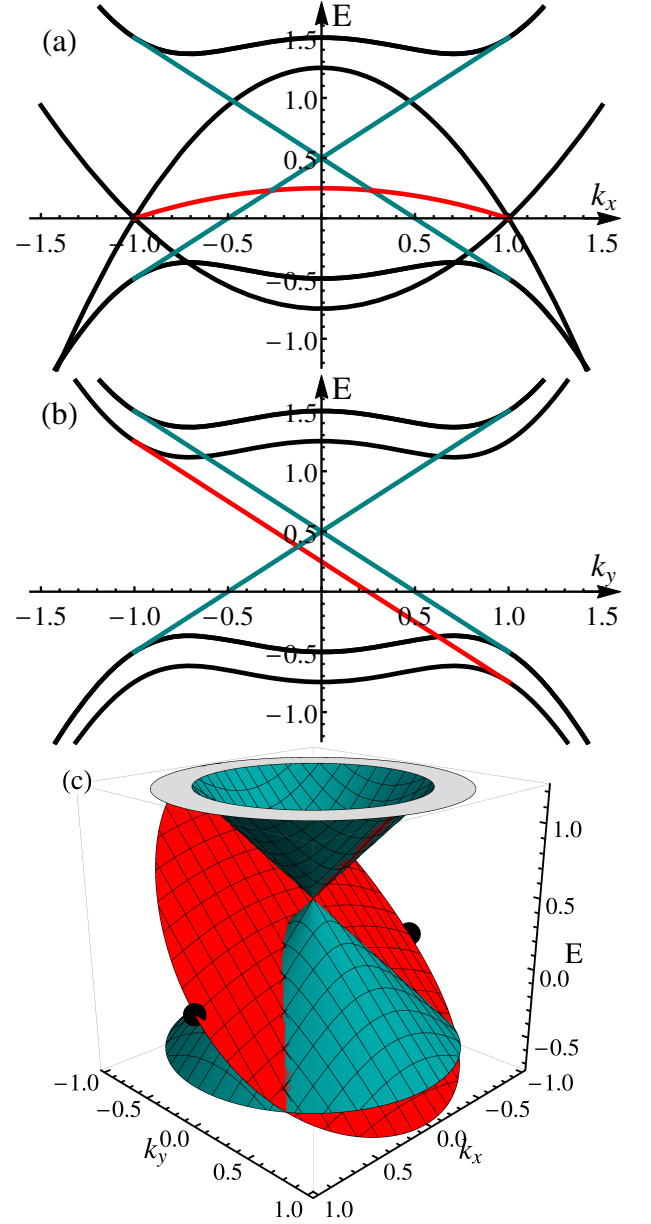


FIG. 3: Bulk (black) and upper surface (red for WSM, cyan for TI) dispersion of the uncoupled TI & WSM model. The two black dots denote the position of the bulk Weyl points. Parameters: $C = \frac{1}{2}$, $M_0 = -1$, $M_1 = 1$, $B = 1$, $k_z = 0$, $\gamma = -\frac{1}{4}$, $A = 1$, $v_y = 1$, $a(k_{\parallel}) = b_1 = 0$, $H_c = \tilde{H}_c$.

surface state, while the other part is maximally coupled, see Eq. (3.9) above. For the lower, hole-like cone, using the parameters in Fig. 4, this direction is $\phi_k = -\frac{\pi}{2}$, thus the negative k_y -axis with $k_x = 0$. The dispersion is then $E = C + Ak_y$ corresponding to the cyan line in Fig. 4 (a) which crosses the other two.

A perturbative calculation can provide some insight into both kinds of Dirac points. We take the surface Hamiltonian, Eq. (3.8), and treat one band as a perturbation to the other two.

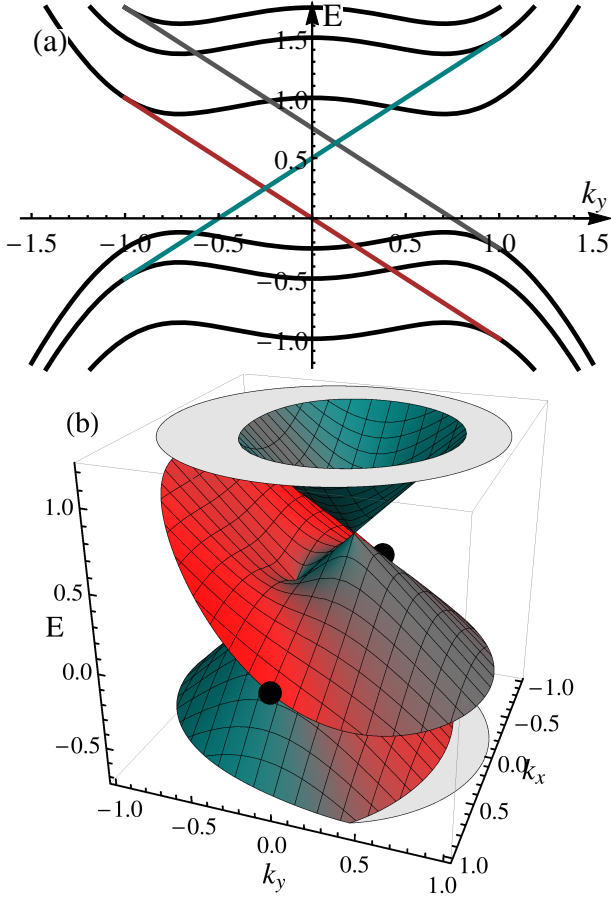


FIG. 4: Bulk (black) and upper surface (red for WSM, cyan for TI) dispersion of the TI & WSM model with real, spin-symmetric coupling. Two Dirac points are visible. Parameters: $C = \frac{1}{2}$, $M_0 = -1$, $M_1 = 1$, $B = 1$, $k_z = 0$, $\gamma = -\frac{1}{4}$, $A = 1$, $v_y = 1$, $a(k_{\parallel}) = \frac{1}{4}$, $b_1 = 0$, $H_c = \tilde{H}_c$.

For the shifted Dirac point one directly finds in 2nd order perturbation theory in the coupling

$$H_D^1 = \begin{pmatrix} C & i\eta A k_- \\ -i\eta A^* k_+ & C \end{pmatrix} + \frac{1}{C - \gamma(M_0 + M_1 k_x^2) - \eta v_y k_y} \begin{pmatrix} |H_c|^2 & H_c \tilde{H}_c^* \\ \tilde{H}_c H_c^* & |\tilde{H}_c|^2 \end{pmatrix}. \quad (4.1)$$

Evidently, a difference in the absolute values of the coupling between the Weyl system and the different spin species of the TI system will open a gap. In the limit of spin degeneracy, we expand Eq. (4.1) for small momenta and find

$$H_D^1 = \begin{pmatrix} C & i\eta A k_- \\ -i\eta A^* k_+ & C \end{pmatrix} + \frac{|a_0|^2}{C - \gamma M_0} \begin{pmatrix} 1 & 1 \\ 1 & 1 \end{pmatrix} + \mathcal{O}(k_{\pm}) \quad (4.2)$$

corresponding to a Dirac cone shifted in energy and momentum by the coupling. For real A the shift occurs in k_y direction as shown in Fig. 4.

The creation of the second Dirac point can be understood from a similar calculation. The perturbative Hamiltonian for this Dirac point is given by

$$H_D^2 = \begin{pmatrix} C - |A| k_{\parallel} & \frac{1}{\sqrt{2}} H_c (1 - e^{i\phi_k^A}) \\ \frac{1}{\sqrt{2}} H_c^* (1 - e^{-i\phi_k^A}) & \gamma(M_0 + M_1 k_x^2) + \eta v_y k_y - |H_c|^2 \frac{1 + \cos(\phi_k^A)}{C + |A| k_{\parallel} - \gamma(M_0 + M_1 k_x^2) - \eta v_y k_y} \end{pmatrix}. \quad (4.3)$$

The off-diagonal elements vanish along the momentum direction $\phi_k = \phi_A + \eta \frac{\pi}{2}$. Thus, Weyl and Dirac surface states are uncoupled in one point. This point becomes the new Dirac point, and setting the diagonal elements of Eq. (4.3) equal, this gives its precise value k_D . For the parameters used in Fig. 4, the Dirac point k_D is on the negative k_y axis, with the Hamiltonian

$$H_D^2 = \begin{pmatrix} C + A(k_D + k_y) & \frac{1}{\sqrt{2}} k_x \left(b_1 + i \frac{a_0}{k_D} \right) \\ \frac{1}{\sqrt{2}} k_x \left(b_1 - i \frac{a_0}{k_D} \right) & C + A(k_D - k_y) + 2f_{di}(k_x, k_y) \end{pmatrix} \quad (4.4)$$

including the distortion $f_{di}(k_x, k_y) = (A - v_y) k_y +$

$$\frac{2b_1(a_0 k_x - x_1 k_D k_y) + A k_D k_y (A - v_y)}{C - (A - v_y) k_D - \gamma M_0} \quad \text{and} \quad k_D = \frac{v_y(C - \gamma M_0) - \sqrt{2a_0^2(A^2 - v_y^2 - 2b_1^2) + (A^2 - 2b_1^2)(C - \gamma M_0)^2}}{A^2 - v_y^2 - 2b_1^2}. \quad \text{The}$$

Dirac point is stable for any real combination of spin-symmetric couplings. A finite distortion $f_{di} \neq 0$ tilts the Dirac cone but does not open a gap.

The number of Dirac points in the surface dispersion can be extended further by a coupling that changes sign as a function of k_x and k_y , e.g. by setting $a_0 > 0$ and $a_2 < 0$. The positions in k -space where the coupling is zero and TI and WSM surface state intersect will then harbor further Dirac points, see Fig. 5.

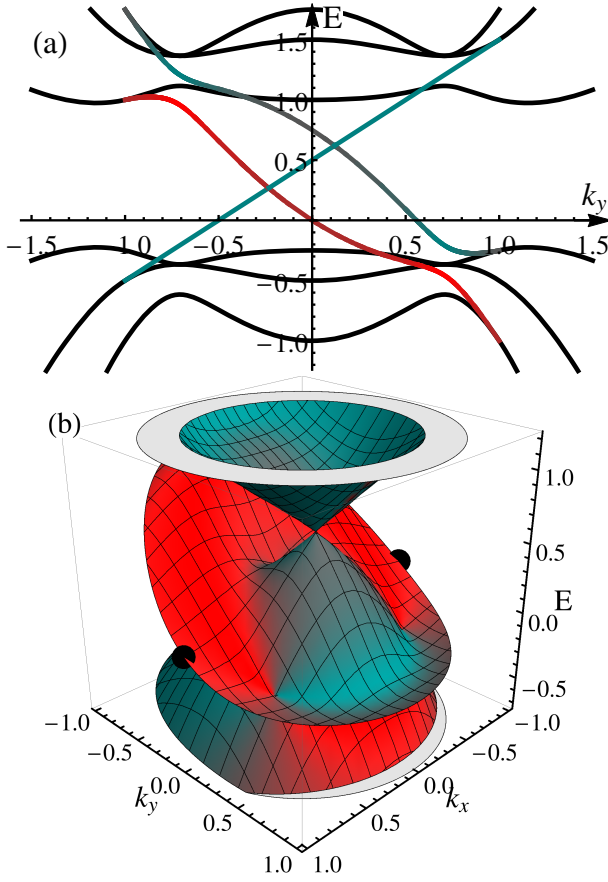


FIG. 5: Bulk (black) and upper surface (red for WSM, cyan for TI) dispersion of the TI & WSM model with a coupling that changes sign. 4 Dirac Points are visible. Parameters: $C = \frac{1}{2}$, $M_0 = -1$, $M_1 = 1$, $B = 1$, $k_z = 0$, $\gamma = -\frac{1}{4}$, $A = 1$, $v_y = 1$, $a_0 = \frac{1}{4}$, $a_2 = -\frac{1}{2}$, $b_1 = 0$, $H_c = \tilde{H}_c$.

C. Spin-asymmetric coupling: Creation of gaps & spin polarization

The spin up and spin down TI bands do not need to have the same coupling to the WSM. If the absolute values are different, $|H_c| \neq |\tilde{H}_c|$, the Dirac points in the surface dispersion are gapped out, see Eq. (4.1) and Fig. 6. The bulk Weyl points are unaffected. The resulting bands are partly spin polarized as shown in Fig. 6. The weaker coupled spin up electrons form a band with the Weyl surface state at medium energies, while the stronger coupled spin down electrons are pushed into the upper and lower band.

D. Phase-shifted coupling: Moving Dirac points, tilting dispersion

Including complex coupling constants, this offers additional ways to alter the bulk and surface spectrum. In general, the dispersion will look much less symmetric compared to the previous, real couplings.

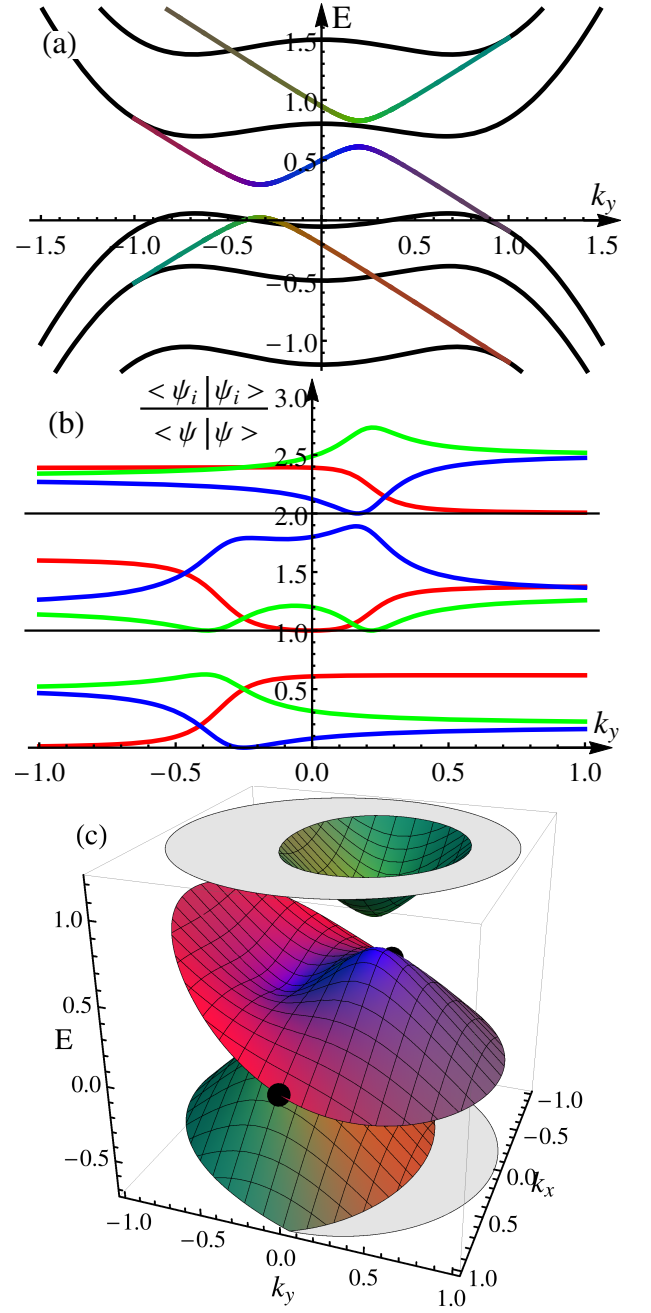


FIG. 6: a) and c): Bulk (black) and upper surface (red for WSM, blue (green) for TI spin up (down)) dispersion of the TI & WSM model with an spin-asymmetric coupling. All Dirac points are gapped. b) Character of the 3 surface bands, shifted for clarity.

Parameters: $C = \frac{1}{2}$, $M_0 = -1$, $M_1 = 1$, $B = 1$, $k_z = 0$, $\gamma = -\frac{1}{4}$, $A = 1$, $v_y = 1$, $a(k_{\parallel}) = \frac{1}{4}$, $\tilde{a}(k_{\parallel}) = \frac{2}{4}$, $b_1 = \tilde{b}_1 = 0$.

Assuming $\tilde{H}_c = H_c$, one can directly conclude from the Hamiltonian in Eq. (3.9) that a complex coupling $A = i$ will lead to two Dirac points lying on the k_x , rather than on the k_y axis as discussed in Sec. IV B. This is confirmed in Fig. 7. One also sees that the bulk Weyl points lie not on the k_x axis, but are rotated by the complex coupling.

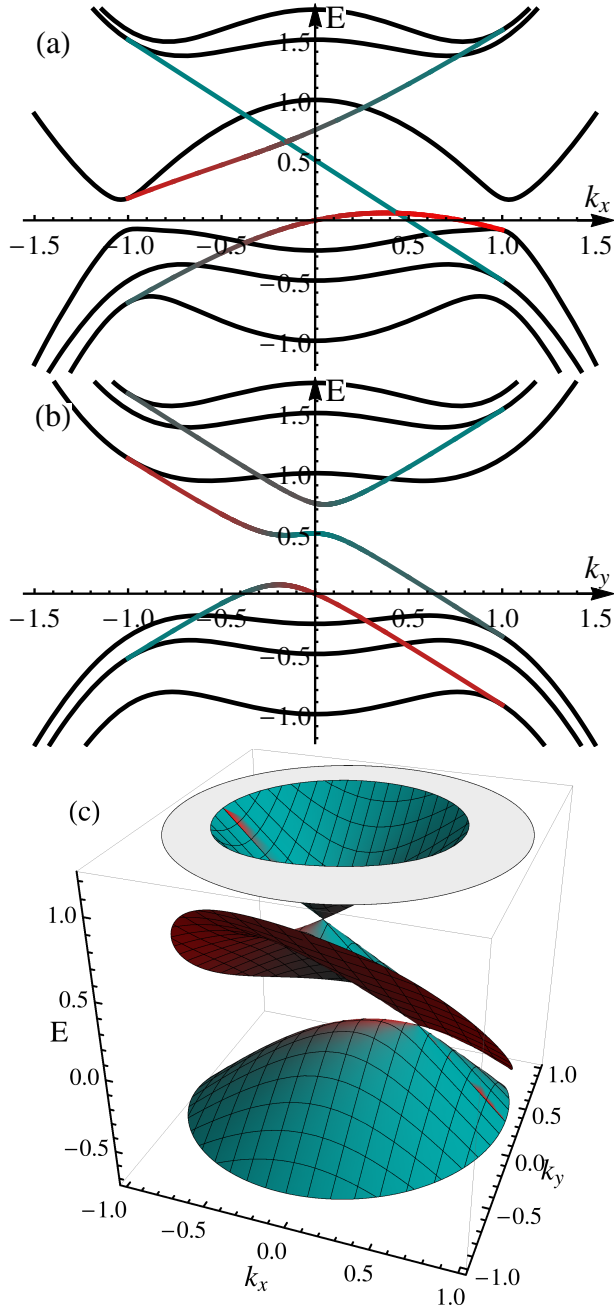


FIG. 7: Bulk (black) and upper surface (red for WSM, cyan for TI) dispersion of the TI & WSM model with a complex coupling. 2 Dirac Points on the k_x axis are visible. Parameters: $C = \frac{1}{2}$, $M_0 = -1$, $M_1 = 1$, $B = 1$, $k_z = 0$, $\gamma = -\frac{1}{4}$, $A = i$, $v_y = 1$, $a(k_{\parallel}) = \frac{1}{4}$, $b_1 = 0$, $H_c = \tilde{H}_c$.

Yet the rotation is much smaller than the $\pi/2$ rotation of the surface Dirac points.

The same effect is obtained by a complex phase difference between the couplings H_c and \tilde{H}_c . It can also undo the rotation induced by $A = i$. Note also that in the spin-symmetric case, already for real and finite $a(k_{\parallel})$ and b_1 the Weyl points are rotated away from the k_x axis. Here

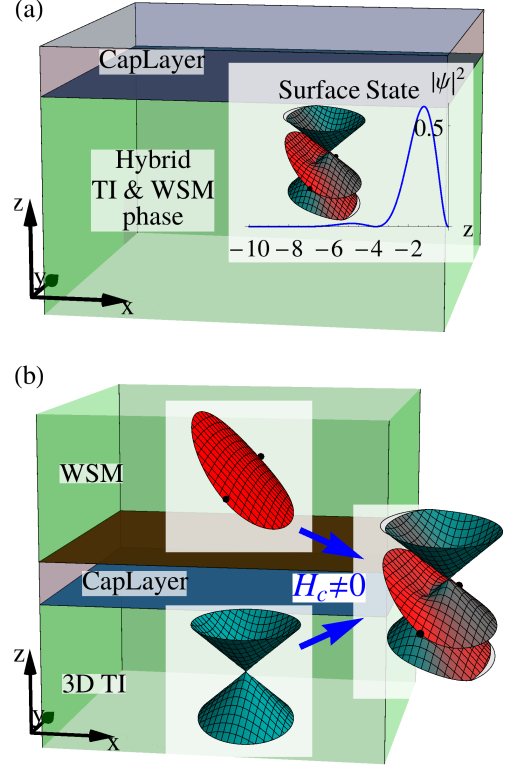


FIG. 8: Possible experimental realizations: (a) Bulk materials being in the combined 3D TI and WSM phase will naturally have hybrid surface states. (b) A heterostructure where TI and WSM phase are adjacent to each other will exhibit hybrid surface states for finite coupling $H_c \neq 0$, provided e.g. by Coulomb interaction or tunneling.

the effective coupling is complex, with a phase changing with k_{\pm} . Supplementing this with a complex $a(k_{\parallel})$, this can again lead to points where the effective coupling is zero, resulting in additional Dirac points like in Sec. IV B.

V. EXPERIMENTAL REALIZATION

We propose two ways to realize the physics of hybrid TI and WSM phases in an experimental setup. First, a material that naturally is in this combined phase will have corresponding surface states, as depicted in Fig. 8 (a). Compressively strained HgTe is a candidate material for this phase: the strain pushes the Γ_8 bands together creating Weyl points²⁶, in addition to the prevailing topological band inversion between Γ_8 and Γ_6 bands. A difference to our calculation is the preserved time-reversal symmetry, leading to 8 Weyl points in HgTe instead of 2. However, if HgTe is doped with Mn the number of Weyl points could be reduced by a (partial) magnetic ordering.

The second realization consists of a WSM in contact with a 3D TI, possibly separated by a thin buffer layer as depicted in Fig. 8 (b). This should lead to a hybrid surface state at the joint boundary. The finite coupling

H_C could be provided by tunneling or Coulomb interaction. While this surface state is not exactly of the form of the Ansatz in Eq. (3.5), the surface Hamiltonian, Eq. (3.8), should still be valid with the modification $\eta = \eta_{TI} = -\eta_W$. As several proposals of TRS-broken WSM with 2 Weyl points are based on magnetically doped 3D TI materials^{33–36}, the fabrication of the described hybrid system should be technically feasible.

VI. CONCLUSION & OUTLOOK

We have analyzed a hybrid system made out of a 3D TI coupled to an inversion symmetric, TRS-broken WSM. In the spirit of a tunnel coupling approach between the two topological phases, the use of a simplified Ansatz made it possible to find analytical solution for the surface states. The resulting surface Hamiltonian Eq. (3.8) is a major result of this paper. The dispersion of the hybrid system shows different phenomena depending on the assumed coupling between WSM and TI. Preserved spin symmetry e.g. leads to the creation of additional Dirac points in the surface dispersion. Breaking of spin symmetry on the other hand, this opens gaps and induces spin polarization in the former Dirac surface cone. As an experimental realization we have presented both strained HgTe, which might naturally be in the discussed hybrid phase, and a heterostructure of TI and WSM. In the latter case, the joint boundary would harbor the interesting hybrid surface state.

There are several directions how to proceed with this research. Looking for measurable consequences, e.g. in transport or spectroscopy, of the new hybrid surface states should be the most immediate one. We expect, for instance, that different Dirac points will give rise to different minima in the conductivity, similar to the graphene case^{47,48}. An extension to time-reversal symmetric WSM is another one. For this, one should use a 4x4 Hamiltonian for the WSM, which offers the possibility of more involved Fermi arcs on the surface, e.g. including spin polarization along the arcs^{49,50}. TaIrTe₄^{30,31} with its 4 Weyl points could be a candidate material for a hybrid system of this kind.

Acknowledgments

We thank C. Brüne, E. M. Hankiewicz, J. M. Mayer and M. Kharitonov for interesting discussions. We acknowledge financial support by the DFG (SPP 1666 and SFB 1170 "ToCoTronics"), the Helmholtz Foundation (VITI) as well as the ENB Graduate school on "Topological Insulators".

Appendix A: Hardwall boundary condition 2x2

In this section, we recap a simple method for calculating exponentially localized boundary states of a 2x2 Hamiltonian following Ref. 41 and references therein. We introduce hard-wall boundary conditions on a half space $z \leq 0$ or $z \geq 0$. Thus, the surface state is localized at $z = 0$ and decays either in direction $z \rightarrow -\infty$ (upper surface) or $z \rightarrow +\infty$ (lower surface). The state should fulfill the eigenvalue equation

$$H\Psi(z) = E\Psi(z) \quad (\text{A1})$$

with $H = \left(h_4(k_{\parallel}^2 + k_z^2) + h_3\right)\tau_3 + h_2k_z\tau_2 + h_1(k_{\pm})\tau_1 + h_0\tau_0$ and h_j being constants or functions of k_{\pm} . The Hamiltonian can represent a topological insulator or Weyl semimetal depending in the chosen h_j .

The general Ansatz for the eigenstate is

$$\Psi_g(z) = \sum_{j \in \{1,2\}} a_j e^{ik_{z,j}z} \psi(k_{\pm}, k_{z,j}), \quad (\text{A2})$$

which could be used to solve for the surface states of Eq. (A1) in the usual manner. Due to the specific structure of our Hamiltonian, we can choose a simplified version of the Ansatz, given by

$$\Psi(z) = (e^{ik_{z,1}z} - e^{ik_{z,2}z}) \psi(k_{\pm}). \quad (\text{A3})$$

It offers the possibility to separate Eq. (A1) into two parts

$$(h_1(k_{\pm})\tau_1 + h_0\tau_0)\Psi(z) = E\tau_0\Psi(z) \quad (\text{A4})$$

$$((h_4(k_{\parallel}^2 + k_z^2) + h_3)\tau_3 + h_2k_z\tau_2)\Psi(z) = 0. \quad (\text{A5})$$

Eq. (A4) is independent of k_z and can be solved for the surface dispersion E , while the solution of Eq. (A5) defines the two quantized values of k_z needed for the surface eigenstate.

Following this procedure, $\psi(k_{\pm}) = f(k_{\pm})\psi_{\pm}$ is taken to be proportional to the eigenstate of the τ_1 Pauli matrix, $\tau_1\psi_{\pm} = \pm\psi_{\pm}$ and

$$\psi_{\pm} = \frac{1}{\sqrt{2}} \begin{pmatrix} 1 \\ \pm 1 \end{pmatrix} \quad (\text{A6})$$

with $f(k_{\pm}) = 1$. Using $\tau_2\psi_{\pm} = \mp i\psi_{\mp}$ and $\tau_3\psi_{\pm} = \psi_{\mp}$, Eq. (A5) reduces to the quadratic equation

$$h_4(k_{\parallel}^2 + k_z^2) + h_3 - \eta i h_2 k_z = 0 \quad (\text{A7})$$

with $\eta = \pm$ the sign from ψ_{\pm} . Solving for k_z , one finds the two solutions

$$ik_{z,\pm} = \frac{1}{2h_4} \left(-\eta h_2 \pm \sqrt{4h_4(h_3 + h_4k_{\parallel}^2) + h_2^2} \right). \quad (\text{A8})$$

In order to obtain a wave function, exponentially decaying of the form of Eq. (A3), both $ik_{z,\pm}$ need a real part of the same sign. This gives us the existence condition

$$h_4 \left(h_3 + h_4 k_{\parallel}^2 \right) < 0. \quad (\text{A9})$$

Depending on the sign of h_2/h_4 and the direction in which the wave function should decay, $z \rightarrow +\infty$ or $z \rightarrow -\infty$, one chooses the corresponding eigenstate ψ_{\pm} , fixing

$$\eta = -\text{sgn} \left(\frac{h_2}{h_4} \right), \text{ top}; \quad \eta = \text{sgn} \left(\frac{h_2}{h_4} \right), \text{ bottom.} \quad (\text{A10})$$

The surface dispersions and wave functions are then given by

$$E^{sur} = h_0 + \eta h_1(k_{\pm}); \quad \Psi(z) = (e^{ik_{z,1}z} - e^{ik_{z,2}z}) \psi_{\eta}. \quad (\text{A11})$$

The localization length is $l_c = \max \left\{ \left| \frac{1}{\Re(ik_{z,\pm})} \right| \right\}$.

The surface solution described in this section fulfills the eigenvalue Eq. (A1) and is thus a valid, non-perturbative eigenstate of the Hamiltonian. Calculating the surface state with the general Ansatz Eq. (A2), this gives the same dispersion as for the simplified Ansatz Eq. (A3) for the TI model in Sec. II A.

-
- ¹ M. Z. Hasan and C. L. Kane, Rev. Mod. Phys. **82**, 3045 (2010).
 - ² X.-L. Qi and S.-C. Zhang, Rev. Mod. Phys. **83**, 1057 (2011).
 - ³ Y. Ando, J. Phys. Soc. Jpn. **82**, 102001 (2013).
 - ⁴ P. Hosur and X. Qi, C. R. Phys. **14**, 857-870 (2013).
 - ⁵ A. M. Turner and A. Vishwanath, arXiv:1301.0330 (2013).
 - ⁶ S. Jia, S.-Y. Xu and M. Z. Hasan, Nat. Mat. **15**, 1140 (2016).
 - ⁷ B. Yan and C. Felser, Annu. Rev. Condens. Matter Phys. **8**, 1-19 (2017).
 - ⁸ H. B. Nielsen and M. Ninomiya, Phys. Lett. B **105**, 219 (1981).
 - ⁹ H. B. Nielsen and M. Ninomiya, Phys. Lett. B **130**, 389 (1983).
 - ¹⁰ S. Murakami, New Journal of Physics **9**, 356 (2007).
 - ¹¹ X. Wan, A. M. Turner, A. Vishwanath and S. Y. Savrasov, Phys. Rev. B **83**, 205101 (2011).
 - ¹² H. Weng, C. Fang, Z. Fang, B. A. Bernevig and X. Dai, Phys. Rev. X **5**, 011029 (2015).
 - ¹³ S.-M. Huang, S.-Y. Xu, I. Belopolski, C.-C. Lee, G. Chang, B. Wang, N. Alidoust, G. Bian, M. Neupane, C. Zhang, S. Jia, A. Bansil, H. Lin and M. Z. Hasan, Nat. Com. **6**, 7373 (2015).
 - ¹⁴ S.-Y. Xu, N. Alidoust, I. Belopolski, Z. Yuan, G. Bian, T.-R. Chang, H. Zheng, V. N. Strocov, D. S. Sanchez, G. Chang, C. Zhang, D. Mou, Y. Wu, L. Huang, C.-C. Lee, S.-M. Huang, B. Wang, A. Bansil, H.-T. Jeng, T. Neupert, A. Kaminski, H. Lin, S. Jia and M. Z. Hasan, Nat. Phys. **11**, 748 (2015).
 - ¹⁵ L. Lu, Z. Wang, D. Ye, L. Ran, L. Fu, J. D. Joannopoulos and M. Soljačić, Science **349**, 622 (2015).
 - ¹⁶ S.-Y. Xu, I. Belopolski, N. Alidoust, M. Neupane, G. Bian, C. Zhang, R. Sankar, G. Chang, Z. Yuan, C.-C. Lee, S.-M. Huang, H. Zheng, J. Ma, D. S. Sanchez, B. Wang, A. Bansil, F. Chou, P. P. Shihayev, H. Lin, S. Jia and M. Z. Hasan, Science **349**, 613 (2015).
 - ¹⁷ B. Q. Lv, H. M. Weng, B. B. Fu, X. P. Wang, H. Miao, J. Ma, P. Richard, X. C. Huang, L. X. Zhao, G. F. Chen, Z. Fang, X. Dai, T. Qian and H. Ding, Phys. Rev. X **5**, 031013 (2015).
 - ¹⁸ B. Q. Lv, N. Xu, H. M. Weng, J. Z. Ma, P. Richard, X. C. Huang, L. X. Zhao, G. F. Chen, C. E. Matt, F. Bisti, V. N. Strocov, J. Mesot, Z. Fang, X. Dai, T. Qian, M. Shi and H. Ding, Nat. Phys. **11**, 724 (2015).
 - ¹⁹ L. X. Yang, Z. K. Liu, Y. Sun, H. Peng, H. F. Yang, T. Zhang, B. Zhou, Y. Zhang, Y. F. Guo, M. Rahn, D. Prabhakaran, Z. Hussain, S.-K. Mo, C. Felser, B. Yan and Y. L. Chen, Nat. Phys. **11**, 728 (2015).
 - ²⁰ L. Huang, T. M. McCormick, M. Ochi, Z. Zhao, M.-T. Suzuki, R. Arita, Y. Wu, D. Mou, H. Cao, J. Yan, N. Trivedi and A. Kaminski, Nat. Mat. **15**, 1155 (2016).
 - ²¹ K. Deng, G. Wan, P. Deng, K. Zhang, S. Ding, E. Wang, M. Yan, H. Huang, H. Zhang, Z. Xu, J. Denlinger, A. Fedorov, H. Yang, W. Duan, H. Yao, Y. Wu, S. Fan, H. Zhang, X. Chen and S. Zhou, Nat. Phys., 3871 (2016).
 - ²² A. Tamai, Q. S. Wu, I. Cucchi, F. Y. Bruno, S. Riccò, T. K. Kim, M. Hoesch, C. Barreateau, E. Giannini, C. Besnard, A. A. Soluyanov and F. Baumberger, Phys. Rev. X **6**, 031021 (2016).
 - ²³ J. Jiang, Z. K. Liu, Y. Sun, H. F. Yang, R. Rajamathi, Y. P. Qi, L. X. Yang, C. Chen, H. Peng, C.-C. Hwang, S. Z. Sun, S.-K. Mo, I. Vobornik, J. Fujii, S. S. P. Parkin, C. Felser, B. H. Yan and Y. L. Chen, arXiv:1604.00139 (2016).
 - ²⁴ N. Xu, Z. J. Wang, A. P. Weber, A. Magrez, P. Bugnon, H. Berger, C. E. Matt, J. Z. Ma, B. B. Fu, B. Q. Lv, N. C. Plumb, M. Radovic, E. Pomjakushina, K. Conder, T. Qian, J. H. Dil, J. Mesot, H. Ding and M. Shi, arXiv:1604.02116 (2016).
 - ²⁵ Y. Sun, S.-C. Wu, M. N. Ali, C. Felser and B. Yan, Phys. Rev. B **92**, 161107(R) (2015).
 - ²⁶ J. Ruan, S.-K. Jian, H. Yao, H. Zhang, S.-C. Zhang and D. Xing, Nat. Comm. **7**, 11136 (2016).
 - ²⁷ J. Ruan, S.-K. Jian, D. Zhang, H. Yao, H. Zhang, S.-C. Zhang and D. Xing, Phys. Rev. Lett. **116**, 226801 (2016).
 - ²⁸ G. Chang, S.-Y. Xu, D. S. Sanchez, S.-M. Huang, C.-C. Lee, T.-R. Chang, H. Zheng, G. Bian, I. Belopolski, N. Alidoust, H.-T. Jeng, A. Bansil, H. Lin and M. Z. Hasan, arXiv:1512.08781 (2015).
 - ²⁹ T. Rauch, S. Achilles, J. Henk and I. Mertig, Phys. Rev. Lett. **114**, 236805 (2015).
 - ³⁰ I. Belopolski, P. Yu, D. S. Sanchez, Y. Ishida, T.-R. Chang, S. S. Zhang, S.-Y. Xu, D. Mou, H. Zheng, G. Chang, G. Bian, H.-T. Jeng, T. Kondo, A. Kaminski, H. Lin, Z. Liu, S. Shin and M. Z. Hasan, arXiv:1610.02013 (2016).
 - ³¹ K. Koepnik, D. Kasinathan, D. V. Efremov, S. Khim, S. Borisenko, B. Büchner and J. van den Brink, Phys. Rev. B **93**, 201101(R) (2016).
 - ³² S. Borisenko, D. Evtushinsky, Q. Gibson, A. Yaresko, T.

- Kim, M. N. Ali, B. Büchner, M. Hoesch and R. J. Cava, arXiv:1507.04847 (2015).
- ³³ A. A. Burkov and L. Balents, Phys. Rev. Lett. **107**, 127205 (2011).
- ³⁴ G. Y. Cho, arXiv:1110.1939 (2011).
- ³⁵ G. Xu, H. Weng, Z. Wang, X. Dai and Z. Fang, Phys. Rev. Lett. **107**, 186806 (2011).
- ³⁶ D. Bulmash, C.-X. Liu and X.-L. Qi, Phys. Rev. B **89**, 081106(R) (2014).
- ³⁷ Z. Wang, M.G. Vergniory, S. Kushwaha, M. Hirschberger, E. V. Chulkov, A. Ernst, N. P. Ong, R. J. Cava and B. A. Bernevig, arXiv:1603.00479 (2016).
- ³⁸ R. Okugawa and S. Murakami, Phys. Rev. B **89**, 235315 (2014).
- ³⁹ A. G. Grushin, J. W. F. Venderbos and J. H. Bardarson, Phys. Rev. B **91**, 121109(R) (2015).
- ⁴⁰ H. Zhang, C.-X. Liu, X.-L. Qi, X. Dai, Z. Fang and S.-C. Zhang, Nat. Phys. **5**, 438 (2009).
- ⁴¹ C.-X. Liu, X.-L. Qi, H. Zhang, X. Dai, Z. Fang and S.-C. Zhang, Phys. Rev. B **82**, 045122 (2010).
- ⁴² K.-Y. Yang, Y.-M. Lu, and Y. Ran, Phys. Rev. B **84**, 075129 (2011).
- ⁴³ T. M. McCormick, I. Kimchi and N. Trivedi, arXiv:1604.03096 (2016).
- ⁴⁴ A. A. Soluyanov, D. Gresch, Z. Wang, Q. Wu, M. Troyer, X. Dai and B. A. Bernevig, Nature **527**, 495 (2015).
- ⁴⁵ G. Sharma, P. Goswami and S. Tewari, arXiv:1608.06625 (2016).
- ⁴⁶ V. Dwivedi and S. T. Ramamurthy, arXiv:1608.01313 (2016).
- ⁴⁷ M. I. Katsnelson, Eur. Phys. J. B **51**, 157 (2006).
- ⁴⁸ J. Tworzydło, B. Trauzettel, M. Titov, A. Rycerz, and C. W. J. Beenakker, Phys. Rev. Lett. **96**, 246802 (2006).
- ⁴⁹ B. Q. Lv, S. Muff, T. Qian, Z. D. Song, S. M. Nie, N. Xu, P. Richard, C. E. Matt, N. C. Plumb, L. X. Zhao, G. F. Chen, Z. Fang, X. Dai, J. H. Dil, J. Mesot, M. Shi, H. M. Weng and H. Ding, Phys. Rev. Lett. **115**, 217601 (2015).
- ⁵⁰ S.-Y. Xu, I. Belopolski, D. S. Sanchez, M. Neupane, G. Chang, K. Yaji, Z. Yuan, C. Zhang, K. Kuroda, G. Bian, C. Guo, H. Lu, T.-R. Chang, N. Alidoust, H. Zheng, C.-C. Lee, S.-M. Huang, C.-H. Hsu, H.-T. Jeng, A. Bansil, T. Neupert, F. Komori, T. Kondo, S. Shin, H. Lin, S. Jia and M. Z. Hasan, Phys. Rev. Lett. **116**, 096801 (2016).